Interplay between cell-adhesion molecules governs synaptic wiring of cone photoreceptors

Yan Cao[a], Yuchen Wang[a], Henry A. Dunn[a], Cesare Orlandi[a,1], Nicole Shultz[b], Naomi Kamasawa[b], David Fitzpatrick[b], Wei Li[c], Christina Zeitz[d], William Hauswirth[e], and Kirill A. Martemyanov[a,2]

[a]Department of Neuroscience, The Scripps Research Institute, Jupiter, FL 33458; [b]Max Planck Florida Institute for Neuroscience, Jupiter, FL 33458; [c]Retinal Neurophysiology Section, National Eye Institute, NIH, Bethesda, MD 20892; [d]Institut de la Vision, Sorbonne Université, INSERM, CNRS, 75012 Paris, France; and [e]Department of Ophthalmology, College of Medicine, University of Florida, Gainesville, FL 32610

Edited by Alex L. Kolodkin, Johns Hopkins University, Baltimore, MD, and accepted by Editorial Board Member Jeremy Nathans August 10, 2020 (received for review May 21, 2020)

Establishment of functional synaptic connections in a selective manner is essential for nervous system operation. In mammalian retinas, rod and cone photoreceptors form selective synaptic connections with different classes of bipolar cells (BCs) to propagate light signals. While there has been progress in elucidating rod wiring, molecular mechanisms used by cones to establish functional synapses with BCs have remained unknown. Using an unbiased proteomic strategy in cone-dominant species, we identified the cell-adhesion molecule ELFN2 to be pivotal for the functional wiring of cones with the ON type of BC. It is selectively expressed in cones and transsynaptically recruits the key neurotransmitter receptor mGluR6 in ON-BCs to enable synaptic transmission. Remarkably, ELFN2 in cone terminals functions in synergy with a related adhesion molecule, ELFN1, and their concerted interplay during development specifies selective wiring and transmission of cone signals. These findings identify a synaptic connectivity mechanism of cones and illustrate how interplay between adhesion molecules and postsynaptic transmitter receptors orchestrates functional synaptic specification in a neural circuit.

retina | cone photoreceptors | synapse formation | cell adhesion | GPCR

Sensory systems update the internal states of an organism based on detected alterations in the surrounding environment (1, 2). This process is essential for the survival of all animals, equipped accordingly with many specialized structures and organs for the detection of a wide spectrum of sensory modalities. Meaningful processing of different sensory inputs requires their segregation into dedicated circuits for transmitting the information into the brain for integration (3, 4).

As life on our planet is powered by light, vision is one of the most fundamental senses. In vertebrates, light is detected by the retina, a specialized neural circuit in the eye and component of the central nervous system (5, 6). Here, all vision-forming inputs originate from two types of light-sensitive neurons—rod and cone photoreceptors—segregated by distinct properties reflecting their unique roles (7–9). Rods are exquisitely light-sensitive but slow-acting and operate only under very low levels of luminance (7, 10, 11). In contrast, cones are fast and have much broader dynamic range (9, 10, 12). Cones are also tuned to different wavelengths of light, enabling color vision, and also segregate their outputs to allow detection of visual features with high acuity (8, 13). These properties endow cone photoreceptors with versatility utilized by most diurnal species for daylight vision.

For the nervous system to optimally utilize the distinct features of cones, their signals need to be distinguished from those generated by rods. To a large extent, this is thought to be achieved by differential wiring of photoreceptors into the retina circuitry, thereby allowing cones to relay their information in a selective manner (14–16). While rods, for the most part, form selective contacts with a single dedicated postsynaptic partner, the rod ON-bipolar cell (RBC), cones largely avoid RBCs and instead make synapses with several types of ON-cone bipolar cells (ON-CBCs) and OFF-cone bipolar cells (OFF-CBCs). We have recently reported that synaptic wiring of rods is mediated by the cell-adhesion molecule ELFN1; however, loss of ELFN1 had no effect on cone synaptic communication (17). This notable specificity led to the hypothesis that a distinct, previously uncharacterized synaptic adhesion molecule(s) may enable selective synaptic wiring of cones for daylight vision.

In this study, we report the identification of the synaptic cell-adhesion molecule ELFN2 as a critical component for the synaptic wiring of cone photoreceptors. We show that ELFN2 acts transsynaptically to recruit and allosterically modulate the key transduction receptor mGluR6 in ON-CBCs. Through the use of multiple genetic animal models, we further uncover an unexpected role of ELFN1 in early development of cone synapses and demonstrate how ELFN1 and ELFN2 cooperate to enable synaptic communication of cone photoreceptors.

Results

Cones Share a Molecularly Similar Wiring Mechanism with Rods. Because loss of rod synapses upon elimination of ELFN1 resulted in selective deficits in mGluR6 targeting in RBCs but not in ON-CBCs (17), we reasoned that cone wiring with ON-CBCs might rely on a distinct transsynaptic association of mGluR6 with an unknown, cone-specific cell-adhesion molecule. To test this hypothesis, we examined the consequence of expressing ELFN1 in cones, where it is not normally detected. These experiments were

Significance

Humans, like most diurnal species, utilize cone photoreceptors to enable daylight vision. They detect color, cover a wide range of light intensities, and sustain fast responsiveness to faithfully sample rapidly changing scenery. All of these features that allow us to accurately see the world depend on the ability of cones to transmit their light-evoked signals to the brain. For this, cones form functional contacts with their downstream neurons—a process known as "synaptic wiring." The molecular mechanisms that mediate establishment of cone synaptic contacts are largely unknown. Our studies fill this gap by identifying a set of molecules involved in functional wiring of cones.

Author contributions: K.A.M. designed research; Y.C., Y.W., H.A.D., C.O., and N.K. performed research; N.S., D.F., W.L., C.Z., and W.H. contributed new reagents/analytic tools; Y.C., Y.W., H.A.D., C.O., and N.K. analyzed data; and Y.C. and K.A.M. wrote the paper.

The authors declare no competing interest.

This article is a PNAS Direct Submission. A.L.K. is a guest editor invited by the Editorial Board.

[1]Present address: Department of Pharmacology and Physiology, University of Rochester Medical Center, Rochester, NY 14642.

[2]To whom correspondence may be addressed. Email: kirill@scripps.edu.

This article contains supporting information online at https://www.pnas.org/lookup/suppl/doi:10.1073/pnas.2009940117/-/DCSupplemental.

First published September 2, 2020.

performed in *Elfn1*$^{-/-}$ mice to concurrently assess the possible role of ELFN1 in the selectivity of photoreceptor wiring. Subretinal injections of virus (recombinant adeno-associated virus; rAAV) containing a mouse *Elfn1* gene under control of a cone-specific promoter (Fig. 1*A*) resulted in selective expression of ELFN1 in cones (Fig. 1*B*). Encouragingly, ELFN1 was specifically targeted to cone terminals identified by cone-arrestin immunostaining and concentrated in the active zones labeled by peanut agglutinin (PNA) (Fig. 1 *B* and *C*). Furthermore, cone-expressed ELFN1 was found to be in close apposition to mGluR6 (Fig. 1*D*). Quantitative analysis revealed a significant increase in synaptic mGluR6 content in apposition to PNA-positive terminals of cones expressing ELFN1 as compared with control ELFN1-negative terminals (Fig. 1*E*). Additionally, expression of ELFN1 resulted in an increase in the number of discrete mGluR6 puncta, thereby suggesting an increase in the number of synaptic contacts between ON-BCs and cones (Fig. 1*E*).

Next, we determined the identity of the ON-BCs responsible for increased wiring with cones. *Elfn1*$^{-/-}$ mice were crossed with an mGluR6-tdTomato reporter line (18) that sparsely labels different ON-BC types and enables tracking their dendritic invaginations into the cone pedicles. Subsequently, protein kinase C α (PKCα) staining was used to distinguish immunopositive RBCs from negative ON-CBCs (Fig. 1*F*). Applying this strategy, we found no evidence of RBC invagination into cone pedicles of *Elfn1*$^{-/-}$ retinas. Viral expression of ELFN1 in cone pedicles also did not significantly alter this pattern and all contacting ON-BCs (40 cells) were classified as ON-CBCs. Together, these results show that while normally ELFN1 is not detected in cones, its overexpression can drive transsynaptic recruitment of mGluR6 to ON-CBC contacts, suggesting that cones utilize an ELFN1-like mechanism for wiring.

Identification of ELFN2 as an mGluR6-Binding Partner in the Retina. To identify endogenously expressed ELFN1-like molecules in cones responsible for the transsynaptic recruitment of mGluR6 on ON-CBCs, we designed a proteomic screen for mGluR6-binding partners, as previous screens in mouse retinas have failed to identify such molecules (17). Reasoning that our chances of detecting relevant mGluR6 partners would be greater in cone-dominant species, we obtained retinas from both ground squirrel and tree shrew species (Fig. 2*A*). Sequence divergence of mGluR6

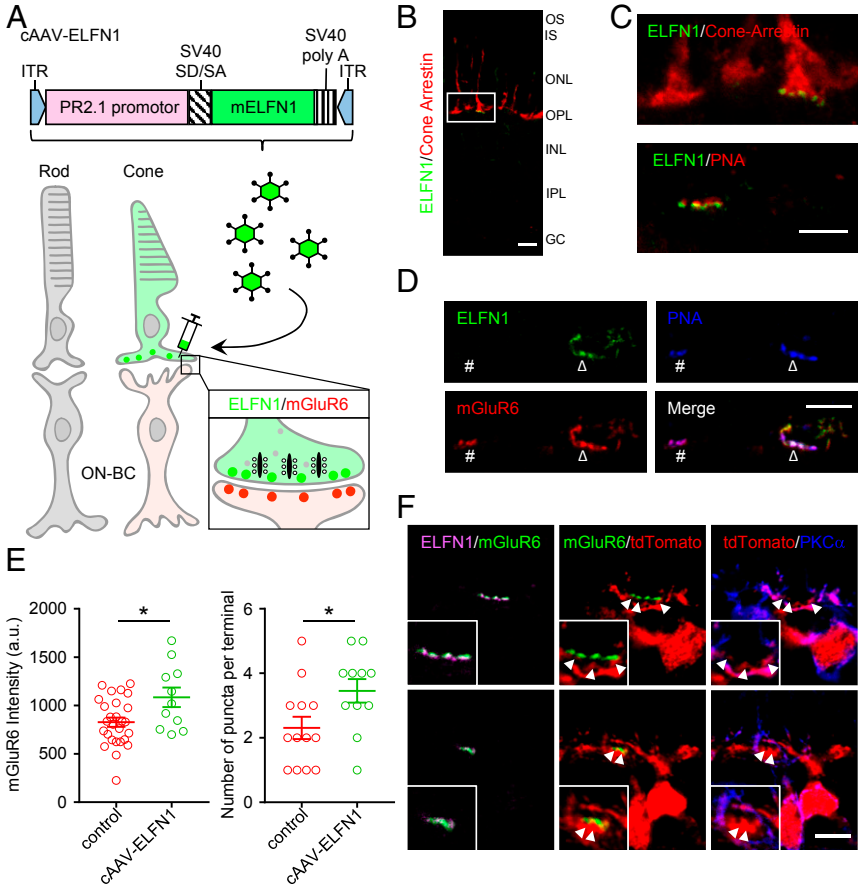

Fig. 1. Virally mediated overexpression of ELFN1 in cones. (*A*) Schematic illustration of a strategy for expressing mouse ELFN1 in cones by subretinal injection of rAAV using cone-specific PR2.1 promotor (cAAV-ELFN1). ITR, inverted terminal repeat; mELFN1, mouse ELFN1; PR2.1, human red opsin promoter; SV40 SD/SA, SV40 splice donor/splice acceptor. (*B*) Selective overexpression of ELFN1 in cones. Retina sections were immunostained for ELFN1 (green) and the cone marker cone arrestin (red). OS, outer segment; IS, inner segment; ONL, outer nuclear layer; OPL, outer plexiform layer; INL, inner nuclear layer; IPL, inner plexiform layer; GC, ganglion cells. (Scale bar, 10 μm.) (*C*) High-power confocal imaging reveals ELFN1 localization in cone terminals. Retina sections were labeled with ELFN1 (green) along with the cone terminal markers cone arrestin (*Upper*, red) or PNA (*Lower*, red). (Scale bar, 5 μm.) (*D*) Effect of ELFN1 overexpression in cones on postsynaptic mGluR6. Retina sections were triple-labeled with ELFN1 (green), mGluR6 (red), and PNA (blue). #, ELFN1 expression-negative terminal (control); Δ, ELFN1 expression-positive terminal (cAAV-ELFN1). (Scale bar, 5 μm.) (*E*) Quantification of the effects of ELFN1 overexpression in cones on mGluR6 content. PNA puncta were used as a mask for the quantification of mGluR6-positive staining. Error bars are SEM. Mean values were obtained from terminals imaged from three mice. *$P < 0.05$, *t* test. a.u., arbitrary units. (*F*) Analysis of cone terminal contacts with dendrites of ON-BC neurons of different classes. tdTomato expression driven by *Grm6* promotor sparsely labeled ON-BCs to trace the dendritic tips of a single cell. ON-RBC projections were identified by positive staining with PKCα. Cone synaptic puncta are indicated by arrowheads. (Scale bar, 5 μm.)

across species necessitated generation of antibodies which could specifically recognize mGluR6 in cone-dominant retinas (*SI Appendix*, Fig. S1*A*), and the resulting antibody could precipitate mGluR6 from ground squirrel and tree shrew but not mouse retinas (*SI Appendix*, Fig. S1*B*). Using this tool, we immunoprecipitated mGluR6 from membrane extracts prepared from ground squirrel and tree shrew retinas on a preparative scale (Fig. 2*A*). Subsequently, mass spectrometry was used to identify coimmunoprecipitating proteins. To account for nonspecific binding, nonimmune immunoglobulin G (IgG)-binding experiments were conducted in parallel and proteins identified in these experiments were excluded. Analysis of proteins specifically copurifying with mGluR6 in both species (Fig. 2*B*) revealed only a few synaptic molecules containing a transmembrane region and also in extracellular segments (Fig. 2*C*). These included the previously characterized rod-expressed ELFN1 (17) and, excitingly, a homologous protein, ELFN2, which had never been characterized in the retina (Fig. 2 *B* and *C*). ELFN2 shares overall topology with ELFN1 including leucine-rich repeats and a fibronectin type 3 domain (Fig. 2*D*).

To determine if ELFN2 was the cone-specific adhesion molecule we were hoping to identify, we next performed a series of experiments characterizing its interaction with mGluR6. First, we were able to reconstitute the binding using heterologous expression in two populations of HEK293T cells transfected separately with either mGluR6 or ELFN2 (Fig. 2*E*). These experiments showed that ELFN2 robustly coimmunoprecipitated mGluR6 with a similar efficiency relative to ELFN1, indicating that ELFN2 and mGluR6 can form a complex in trans. Next, we studied the impact of transcellular ELFN2 binding on mGluR6 activity, suggested by analogous interactions of ELFN2 with other group III members of

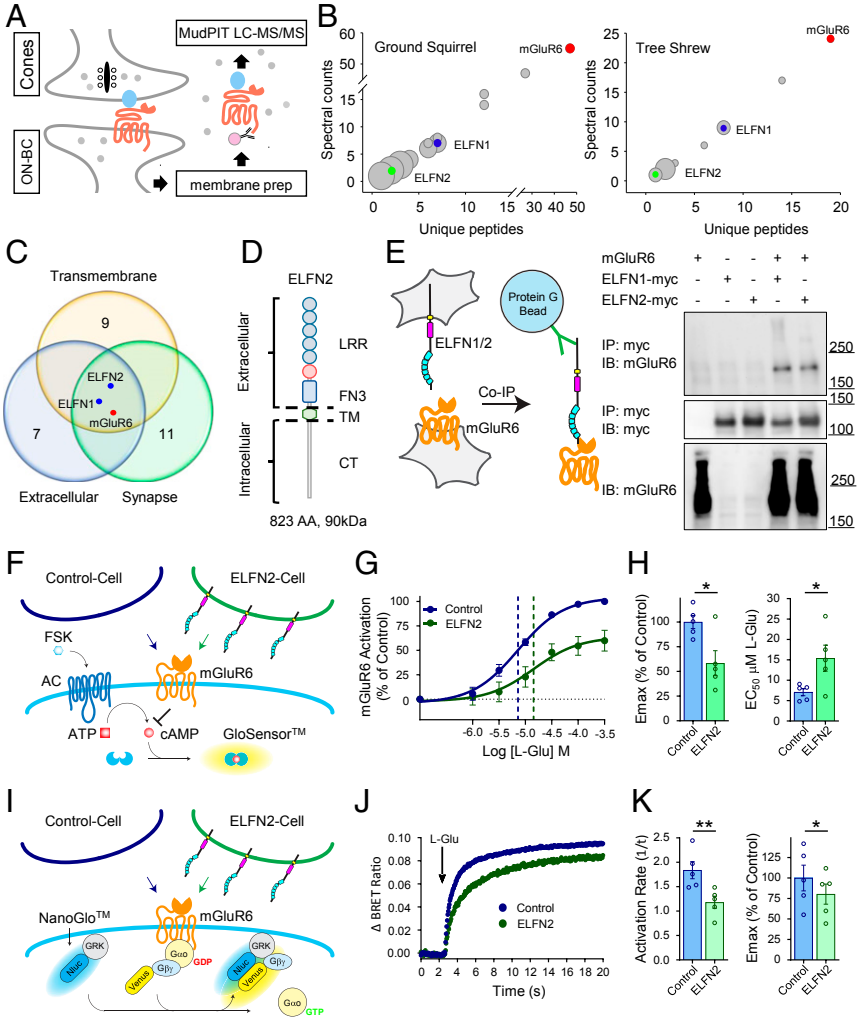

Fig. 2. ELFN2 is a binding partner of mGluR6 in cone-dominant retinas. (*A*) Schematics of the proteomic strategy for identification of mGluR6-interacting proteins. LC-MS/MS, liquid chromatography-tandem mass spectrometry. (*B*) Analysis of proteins coimmunoprecipitated with mGluR6 as identified by mass spectrometry in ground squirrel (*Left*) and tree shrew (*Right*) retina. (*C*) Categorical classification of mGluR6-binding partners by DAVID functional annotation. (*D*) Domain composition of ELFN2. The protein contains extracellular leucine-rich repeats and fibronectin type 3 (FN3) domains, the transmembrane segment (TM), and intracellular C terminus (CT). (*E*) ELFN2 and mGluR6 interact in trans. Proteins were coimmunoprecipitated following transient expression in separate HEK293 cells followed by Western blot detection. IB, immunoblotting. (*F*) ELFN2 modulates pharmacological properties of mGluR6 in trans. Schematic representation of transcellular GPCR signaling assay utilizing cAMP pGloSensor in mGluR6-expressing cells exposed to control or ELFN2-expressing cells that lack the biosensor. (*G*) Dose–response curves plotted for the identical mGluR6- and biosensor-expressing cell populations, differing only by exposure to either control or ELFN2-expressing cells. (*H*) Quantification of ELFN2 effects on mGluR6 response parameters: maximal efficacy (E_{max}) and half-maximal effective concentration (EC_{50}) for L-glutamic acid. $^*P < 0.05$, paired *t* test. (*I*) Transcellular interactions with ELFN2 alter G protein-coupling efficiency of mGluR6. Schematic representation of transcellular GPCR-Gαo signaling assay utilizing real-time kinetic BRET strategy in mGluR6-expressing cells cocultured with control or ELFN2-expressing cells. (*J*) ELFN2-induced changes in kinetic properties of mGluR6 signaling to Gαo. (*K*) Quantification of ELFN2 effects on mGluR6-mediated Gαo activation rate and maximal response amplitudes (E_{max}) for L-glutamic acid. $^{**}P < 0.01$, $^*P < 0.05$, paired *t* test.

the mGluR family in the brain (19). Initially, we used cyclic adenosine monophosphate (cAMP) as a readout for mGluR6 activity, studying it in a transcellular format where mGluR6 and ELFN2 were segregated to different cell populations (Fig. 2*F*). Coculturing ELFN2-expressing cells, but not control cells, with cells expressing mGluR6 and cAMP reporters revealed a significant modulation of both efficacy and potency of mGluR6 responses to glutamate (Fig. 2 *G* and *H*) and its synthetic agonist L-AP4 (*SI Appendix*, Fig. S1 *C–E*). Dissecting the mechanism of this effect using bioluminescence resonance energy transfer (BRET) sensors that directly report G-protein activation, we found that coculturing with ELFN2-expressing cells directly inhibited mGluR6-mediated activation of Gαo, a G protein that transmits mGluR6 signals in ON-BCs (Fig. 2*I*). This transcellular interaction critically altered both the activation kinetics, which serve as a proxy for potency, and maximal amplitude, which is a measure of efficacy (Fig. 2 *J* and *K*). Importantly, ELFN2 had no effect on mGluR6 desensitization following its prolonged activation by glutamate (*SI Appendix*, Fig. S1 *F–K*), suggesting the observed changes in both potency and efficacy are attributable to transcellular allosteric modulation of receptor function rather than altered receptor trafficking. Together, this evidence supports a model in which ELFN2 directly associates with mGluR6 and serves as its direct allosteric modulator in trans.

ELFN2 Is Expressed by Cone Photoreceptors and Hierarchically Integrated into Their Synapses. To characterize ELFN2 expression and distribution, we stained retina cross-sections with anti-ELFN2 antibodies. We found ELFN2 protein to be prominently present across the entire outer plexiform layer (OPL) in both tree shrew and ground squirrel (*SI Appendix*, Fig. S2*A*), where it was associated with the synaptic markers (*SI Appendix*, Fig. S2*B*). We have also observed immunoreactivity for ELFN2 protein in the inner plexiform layer (INL). A rod-dominant mouse retina exhibited pronounced staining for the ELFN2 protein in the OPL with islands of intense signal reminiscent of its presence in cone pedicles (Fig. 3*A*). To study the cell specificity of ELFN2 expression in photoreceptors, we conducted fluorescence in situ hybridization which also showed sparse distribution of *Elfn2* messenger RNA (mRNA) (*SI Appendix*, Fig. S2*C*). Double labeling showed that all *Elfn2* signals were confined to cells also expressing cone marker *Gnat2* and absent in the surrounding rods (Fig. 3*B*). These results point to selective expression of *Elfn2* in cones and not in rods. Consistent with these data,

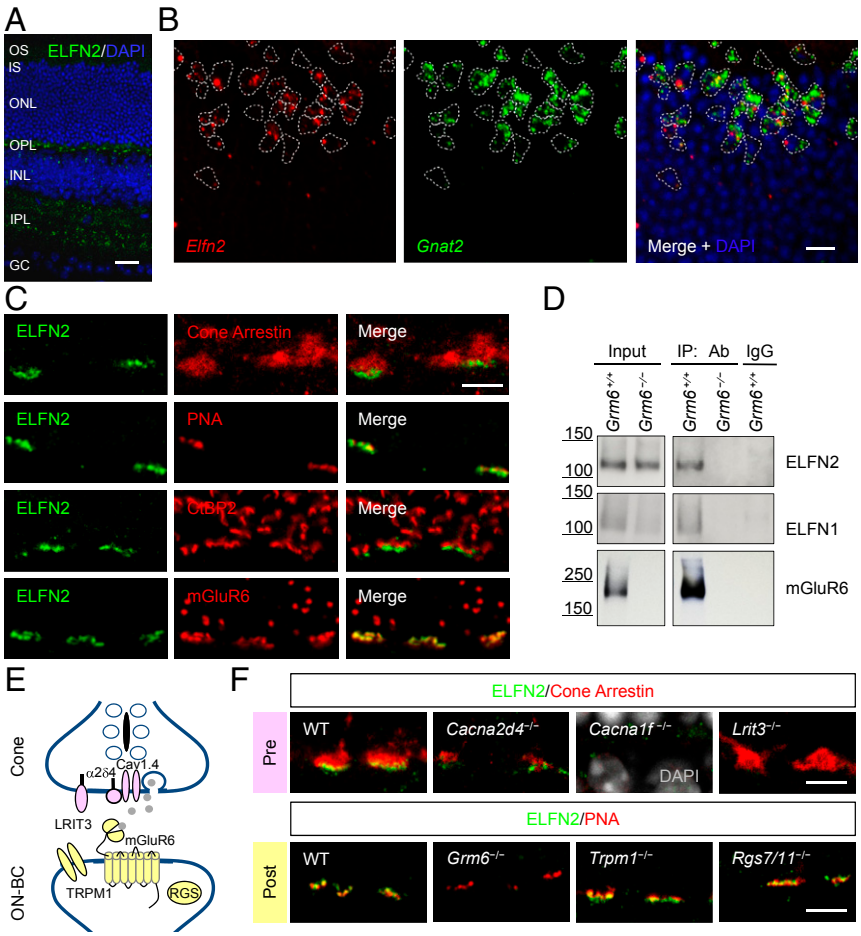

Fig. 3. ELFN2 is a synaptic protein localized in cone terminals. (*A*) Analysis of ELFN2 protein localization in mouse retina cross-sections by immunohistochemistry with a specific anti-ELFN2 antibody. (Scale bar, 25 μm.) (*B*) Cellular specificity of ELFN2 expression revealed by double in situ hybridization for *Elfn2* mRNA (red) with mRNA for cone-specific Gαt2 (green). (Scale bar, 10 μm.) (*C*) Selective localization of ELFN2 at the synapse terminals of cone photoreceptors. Mouse retina cross-sections were costained with cone terminal markers cone arrestin and PNA, presynaptic photoreceptor marker (CtBP2), and postsynaptic ON-BC marker (mGluR6). (Scale bar, 5 μm.) (*D*) Coimmunoprecipitation of mGluR6 and ELFN2 from mouse retinas as detected by Western blotting. Samples from retinas of a *Grm6*$^{-/-}$ mouse or pulled down from nonimmune IgG lacking mGluR6 antibodies are used as specificity controls. (*E*) Schematic illustration of the identity and localization of key molecules at photoreceptor synapses analyzed in the experiments. (*F*) Effect of eliminating key synaptic molecules on expression and localization of ELFN2 at cone synapses. Retinas of the indicated knockout mice were analyzed. (Scale bars, 5 μm.)

higher-power confocal microscopy of the OPL revealed that all ELFN2 protein was localized at the base of cone terminals labeled with cone arrestin (Fig. 3*C*). ELFN2 staining also coincided with the cone-specific active zone marker PNA. Within the cone terminals, ELFN2 coclustered with photoreceptor ribbons in direct apposition to postsynaptic mGluR6, characteristically contacting cone terminals in the lower sublamina of the OPL. Notably, we found no overlap between ELFN2 and the dendritic tips of RBCs that contact rods (*SI Appendix*, Fig. S2*D*).

Next, we confirmed the interaction between ELFN2 and mGluR6 in mouse retinas by coimmunoprecipitation (IP) using anti-mouse mGluR6 antibodies. These experiments showed that ELFN2 was specifically present in the mGluR6 IP eluates in wild-type retinas and not in *Grm6*$^{-/-}$ or IgG controls (Fig. 3*D*).

To understand the place of ELFN2 in the hierarchy of synaptic organization, we next determined how it is influenced by the disruption of pre- and postsynaptic elements. We found that synaptic accumulation of ELFN2 was reduced in cone terminals of *Lrit3* and *Cacna1f* knockout retinas but detectable upon elimination of α2δ4 protein (Fig. 3*F*). Consistent with transsynaptic stabilization of ELFN2–mGluR6 complexes, elimination of mGluR6 dramatically decreased ELFN2 content in cone terminals. In contrast, loss of TRPM1 or RGS proteins did not affect ELFN2 synaptic targeting in cones (Fig. 3*F*). Taken together, these results indicate that ELFN2 is a cone-specific synaptic molecule that transsynaptically scaffolds mGluR6 on the dendritic tips of ON-CBCs and is uniquely integrated in the synaptic milieu of cone pedicles.

Knockout of ELFN2 Has No Discernable Structural or Functional Effects but Activates ELFN1 Expression in Cones. To further investigate the role of ELFN2 in the retina, we used a null mutant mouse line (*Elfn2*$^{-/-}$), where the entire coding sequence of *Elfn2* was eliminated (Fig. 4*A*). Indeed, this resulted in complete loss of ELFN2 immunoreactivity upon immunohistochemical staining of retina sections and loss of positive bands in Western blotting of retina lysates, indicating complete loss of ELFN2 expression and also confirming specificity of the antibody we used to detect ELFN2 (Fig. 4 *B* and *C*). Contrary to our expectations, elimination of ELFN2 did not affect the expression levels of key molecules involved in synaptic communication of photoreceptors including mGluR6, TRPM1, Gαo, and the GAP complex, as analyzed by Western blotting (Fig. 4*C* and *SI Appendix*, Fig. S3*A*). We also detected no changes in the molecular architecture of the retinas lacking ELFN2, with all of the synaptic signaling components examined being appropriately targeted to the synaptic sites in both rod and cone photoreceptors (*SI Appendix*, Fig. S3*B*).

Analysis of retina light responses by electroretinography (ERG) revealed no changes in either a or b waves under either scotopic or photopic conditions. The amplitudes and kinetic parameters of the light responses in *Elfn2*$^{-/-}$ were indistinguishable from wild-type (WT) littermates across a range of eliciting light intensities in dark-adapted animals and upon background adaptation (Fig. 4 *D*–*I* and *SI Appendix*, Fig. S3*C*). These results indicate that loss of ELFN2 alone does not impact synaptic transmission of either rod or cone photoreceptors.

Strikingly, during our immunohistochemical analysis of retina architecture, we found that cone pedicles of *Elfn2*$^{-/-}$ mice uniquely contained ELFN1 that was undetectable in cones of WT retinas (Fig. 4*J* and *SI Appendix*, Fig. S3*B*). This cone ELFN1 immunoreactivity in *Elfn2*$^{-/-}$ retinas recapitulated localization of ELFN2 in WT cones, demonstrating close association with PNA-positive active zones in immediate apposition to mGluR6 clusters of the ON-CBCs in the lower OPL sublamina (Fig. 4*J*). Thus, lack of an observed phenotype in *Elfn2*$^{-/-}$ mice might be obscured by cone-specific activation and synaptic compensation from ELFN1 whose expression in cones was triggered by the loss of ELFN2.

Developmental Dynamics of ELFN1 and ELFN2 Interplay in Cone Synapses. To better understand the relationship between ELFN1 and ELFN2 in cones, we studied developmental dynamics of their expression and their interdependence during the time frame of photoreceptor synaptogenesis. Strikingly, we found that at early stages of development (postnatal day 7; P7), ELFN1 protein was in fact present in cone synapses (Fig. 5 and *SI Appendix*, Fig. S4). However, we observed that the levels of ELFN1 progressively declined as the synapses matured, falling to barely detectable levels in fully developed retinas at P21. This trajectory was markedly altered in *Elfn2*$^{-/-}$ retinas, where ELFN1 underwent substantial up-regulation in cone synapses, instead reaching peak levels upon completion of synaptogenesis at P17 before stabilizing to adult levels at P21.

The dynamics of ELFN2 expression were markedly different (Fig. 5 and *SI Appendix*, Fig. S4). Following initial up-regulation at the peak of cone synapse formation at P11, its levels remained rather steady throughout development. Interestingly, in *Elfn1*$^{-/-}$ retinas, the levels of ELFN2 continued to rise, reaching the plateau later, around P17. These observations suggest that ELFN1 and ELFN2 expression is interdependent and temporally segregated throughout retinal development, acting during different stages in cone synapse ontogeny, switching from ELFN1-abundant early synapses to ELFN2-abundant mature synapses.

Changes in ELFN1 and ELFN2 Content Alter Synaptic Transmission of Cone Photoreceptors. To test the possibility that induction of ELFN1 expression may functionally compensate for the loss of ELFN2, we attempted generating a line of constitutive double-knockout mice by crossing *Elfn1*$^{-/-}$ and *Elfn2*$^{-/-}$ strains. However, this was not successful due to embryonic lethality associated with concurrent elimination of both proteins, reinforcing the possibility of their coinvolvement in many other circuits essential for survival across the nervous system. Thus, we generated a strain for conditional elimination of *Elfn1*-flanking exon 2 by loxP sites (*Elfn1*$^{flox/flox}$; Fig. 6*A*). In the resulting homozygous *Elfn1*$^{flox/flox}$ mice, the synaptic content of ELFN1 was decreased (*SI Appendix*, Fig. S5 *A* and *B*). However, this reduction did not result in lower postsynaptic recruitment of mGluR6 (*SI Appendix*, Fig. S5*C*). Furthermore, the content of all other proteins examined, including components of the calcium channel and GAP complexes in the synapses of rods and cones, were normal and indistinguishable from WT retinas. Consistent with these observations, the light responses of *Elfn1*$^{flox/flox}$ mice as measured by ERG were not different from WT mice (*SI Appendix*, Fig. S5 *D*–*J*), making it a suitable model for studying conditional elimination of ELFN1.

We next generated and characterized conditional *Elfn1*$^{flox/flox}$ *Elfn2*$^{-/-}$ double-knockout (*cDKO*) mice, which were now viable. As before, we did detect ELFN1 induction in cone synapses of *cDKO* retinas (Fig. 6*B*). We found that mGluR6 was reduced in *cDKO* cone synapses, suggesting that combined ELFN1/ELFN2 content in cones in this model fell below the critical threshold needed for normal transsynaptic recruitment of mGluR6 (Fig. 6 *B* and *C*). This change was specific, as we did not detect significant alteration in localization of other synaptic signaling molecules in *cDKO* retinas (*SI Appendix*, Fig. S6*A*). We further detected a small but significant reduction in the amplitude of photopic ERG b waves in *cDKO* mice (Fig. 6 *D* and *E*), indicating that decrease in mGluR6 controlled by ELFN1/2 in cones was sufficient to functionally impact synaptic transmission to ON-CBCs.

To further reduce the levels of ELFN1/2, we crossed the *Elfn1*$^{flox/flox}$*Elfn2*$^{-/-}$ mouse with the inducible pan-neuronal Cre driver line *CAG*^{CreERT2} followed by tamoxifen induction in adults to avoid embryonic lethality (*iDKO*) (Fig. 6*A*). Cre-mediated deletion reduced the ELFN1 content in cones to barely detectable levels (Fig. 6*F* and *SI Appendix*, Fig. S6 *B* and *C*). This was accompanied by further reduction in mGluR6 levels in cone

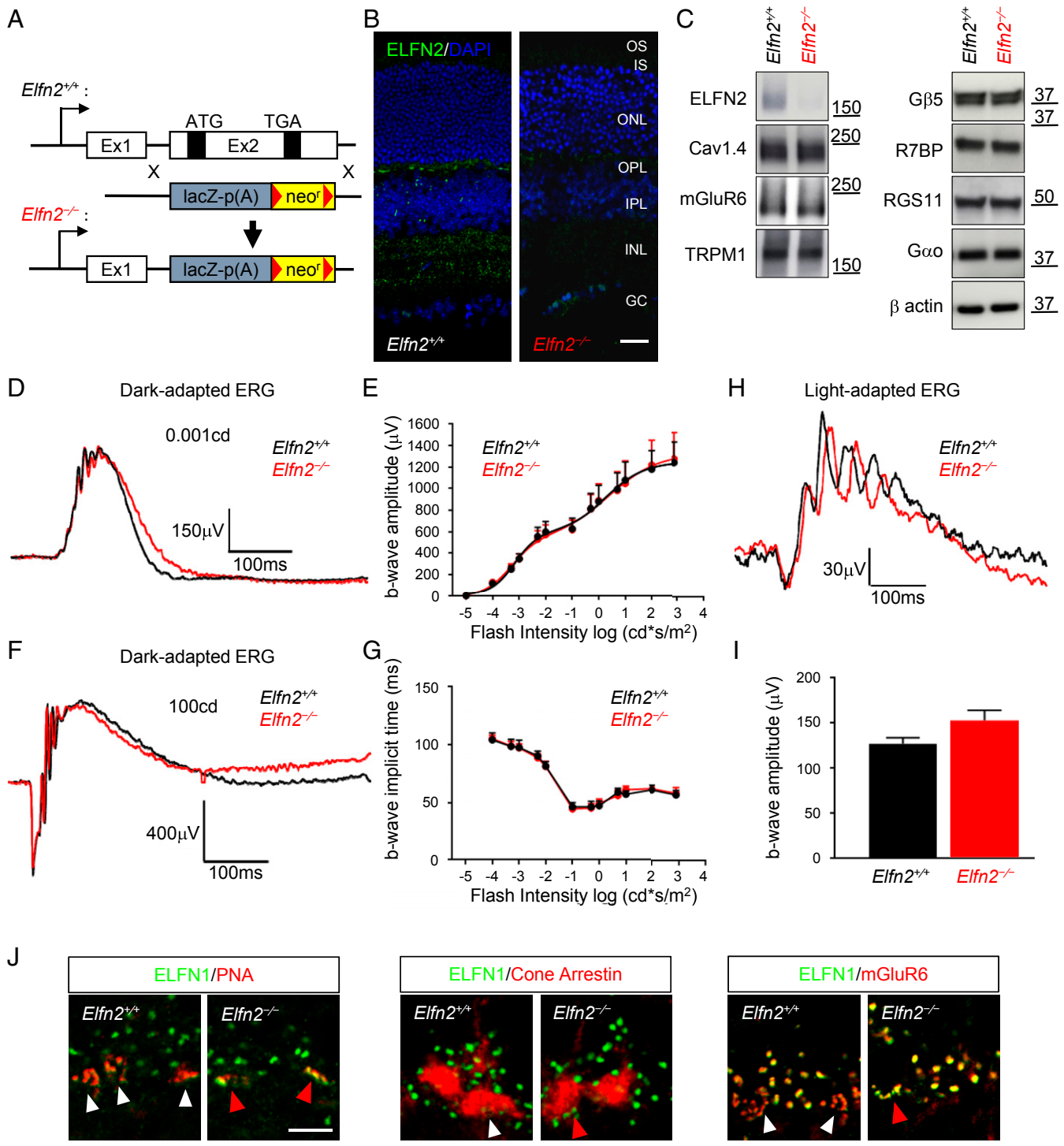

Fig. 4. Impact of ELFN2 loss on synaptic organization and function. (*A*) Schematics of the strategy for disrupting *Elfn2* in mice. (*B*) Elimination of ELFN2 staining (green) in *Elfn2*$^{-/-}$ retinas. (Scale bar, 25 μm.) (*C*) Effect of ELFN2 elimination on the expression of major photoreceptor synaptic proteins analyzed by Western blotting of retina lysates. (*D*) Representative ERG traces elicited by a scotopic flash of 0.001 cd*s/m^2 (~0.6 R* per rod) to activate the primary rod pathway only. (*E*) Dose–response plot of maximal dark-adapted ERG b-wave amplitudes from *Elfn2*$^{+/+}$ (n = 5) and *Elfn2*$^{-/-}$ (n = 4) mice plotted against their eliciting flash intensities. Data are represented as mean ± SEM. (*F*) Representative ERG traces of responses to a photopic flash of 100 cd*s/m^2 (~58,000 R* per rod) to activate both rod and cone pathways. (*G*) Dose–response of maximal b-wave time to peak from *Elfn2*$^{+/+}$ and *Elfn2*$^{-/-}$ mice plotted against their eliciting flash intensities. Data are represented as mean ± SEM. (*H*) Representative ERG traces of responses to a photopic flash of 100 cd*s/m^2 (~58,000 R* per rod) under a 32 cd*s/m^2 (~18,500 R* per rod per second) light background to activate the cone pathway only. (*I*) Quantification of b-wave amplitude of light-adapted ERG in *Elfn2*$^{+/+}$ (n = 5) and *Elfn2*$^{-/-}$ (n = 4). Data are represented as mean ± SEM. (*J*) Analysis of the effect of ELFN2 loss on synaptic content of ELFN1 in cone terminals. Retina cross-sections were double-immunostained with antibody against ELFN1 (green) and presynaptic cone terminal marker PNA (red) or cone arrestin (red), or double-stained with postsynaptic receptor mGluR6 (red). (Scale bar, 5 μm.) There were no significant genotype differences in data reported in *D*, *F*, *I*, and *J*, $P > 0.05$ based on multiple t test.

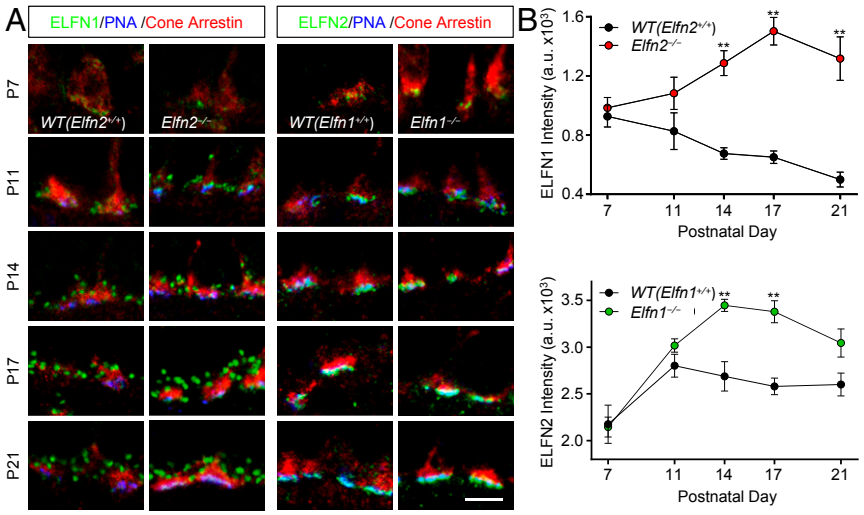

Fig. 5. Developmental dynamics of ELFN1 and ELFN2 accumulation at cone synapses. (*A*) Immunostaining for ELFN1 and ELFN2 in retina cross-sections from mice at different developmental stages. Cone arrestin and PNA were used to identify cone terminals. (Scale bar, 5 μm.) (*B*) Quantification of changes in content of ELFN1 and ELFN2 in cone synapses during development. Mean fluorescence intensity from 10 puncta per retina section was measured from three to six images per retina collected from two separate mice at each developmental time point. Data are represented as mean ± SEM; $n = 12$ to 18. $^{**}P < 0.01$, two-way ANOVA followed by Sidak's multiple-comparisons test.

synapses to 12.3% of the amount present in *cDKO* (Fig. 6 *F* and *G*). Analysis of cone synaptic transmission in *iDKO* mice by ERG revealed dramatic reduction of the photopic b wave relative to *cDKO* mice (Fig. 6 *H* and *I*). Yet, when compared with $Trpm1^{-/-}$ mice in which synaptic transmission of photoreceptors is completely ablated, the *iDKO* mice still showed a discernable residual b wave. The incomplete elimination of ELFN1 is likely explained by a weak activity of the $CAG^{CreERT2}$ driver in photoreceptors. Together, the comparative analysis of *cDKO* and *iDKO* models revealed that synaptic mGluR6 content and resulting generation of the postsynaptic response are titrated by availability of presynaptic ELFN1 proteins in mature retinas and that even small amounts of ELFN1 can enable some level of functional wiring of photoreceptors.

Complete Inactivation of Both ELFN1 and ELFN2 Abolishes Synaptic Transmission of Photoreceptors. In an attempt to completely eliminate both ELFN1 and ELFN2, we crossed $Elfn1^{flox/flox}Elfn2^{-/-}$ mice with the $Pcdh21^{Cre}$ line, a constitutive driver active in rod and cone photoreceptors (Fig. 7*A*). The resulting $Elfn1^{flox/flox}Elfn2^{-/-}$-$Pcdh21^{Cre}$ mice (*pDKO*) was expected to delete ELFN1 specifically in photoreceptors in addition to global elimination of ELFN2 (Fig. 7*B*). Indeed, we found complete elimination of ELFN1 immunoreactivity in cone synapses of *pDKO* retinas. Concomitantly, mGluR6 puncta at cone synapses were also completely absent (Fig. 7*B*). The loss of mGluR6 was paralleled by a prominent reduction in accumulation of several postsynaptic proteins in cone synapses known to be dependent on mGluR6, including RGS11 and GPR179, but not presynaptic mGluR6-independent proteins (Fig. 7*B* and *SI Appendix*, Fig. S7*A*). Interestingly, we found the cone-enriched synaptic cell-adhesion molecule LRIT3 to be significantly reduced yet present at cone synapses, suggesting that ELFNs and LRITs could cooperate during cone synaptic development (Fig. 7*B* and *SI Appendix*, Fig. S7*B*).

Most strikingly, evaluation by ERG revealed complete lack of photopic b wave amid normal a wave, indicating that light responses of cone photoreceptors were intact but their synaptic communication with ON-BCs was abolished (Fig. 7*C*). These changes were paralleled by the expected loss of scotopic b wave (*SI Appendix*, Fig. S7*D*), given the critical role of ELFN1 in synaptic transmission of rod signals. This phenotype was no different from the responses seen in $Trpm1^{-/-}$ mice and other models with complete loss of synaptic transmission (20), typically referred to as nob (no b wave). Thus, we have determined that combined contributions of both ELFN1 and ELFN2 in cones are absolutely required for recruitment of postsynaptic signaling complexes and synaptic transmission of cone signals.

Because elimination of ELFN1 disrupted physical synapse formation of rod photoreceptors (17), we next asked whether ELFN proteins play a role in establishment of synaptic contacts of cones as well. Examination of cone pedicles in *pDKO* retinas by transmission electron microscopy revealed that their overall morphology was normal with multiple easily identifiable ribbons and adjacent processes of horizontal cells (Fig. 7*D*). We further found abundant evidence for the presence of the invaginating contacts typically made by the ON-CBCs. Quantitative analysis did not reveal differences between *pDKO* and their Cre-negative control littermates (*cDKO*) in the number of invaginating ON-CBC contacts (Fig. 7*E*). We also observed a similar number of flat contacts at the base of cone pedicles, typically formed by the OFF-BCs between *pDKO* (329 contacts in 99 cone pedicles) and *cDKO* (304 contacts in 84 cone pedicles) (Fig. 7*D*). Control experiments confirmed the expected disruption of rod synapses in *pDKO* retinas (*SI Appendix*, Fig. S7*C*) similar to what was observed upon constitutive elimination of ELFN1 (17). These results suggest that elimination of ELFN1/2 primarily affects functional rather than structural wiring of cones with their postsynaptic partners.

This normal synaptic morphology suggests that observed deficits in synaptic transmission are driven by reduction in mGluR6 function. To confirm this connection, we performed comparative analysis of several mouse models that produce varying degrees of ELFN protein loss. We found that changes in the synaptic content of ELFNs at cone synapses nearly perfectly correlated with the synaptic accumulation of mGluR6: The more ELFN proteins present, the more mGluR6 was recruited to cone synapses (Fig. 7*F*). Importantly, the mGluR6 synaptic content tightly correlated with the strength of the synaptic transmission as evidenced by ERG b-wave amplitudes (Fig. 7*F*). These observations suggest that ELFN proteins are essential in the functional wiring of cone photoreceptors by regulating the extent of the transsynaptic recruitment of mGluR6.

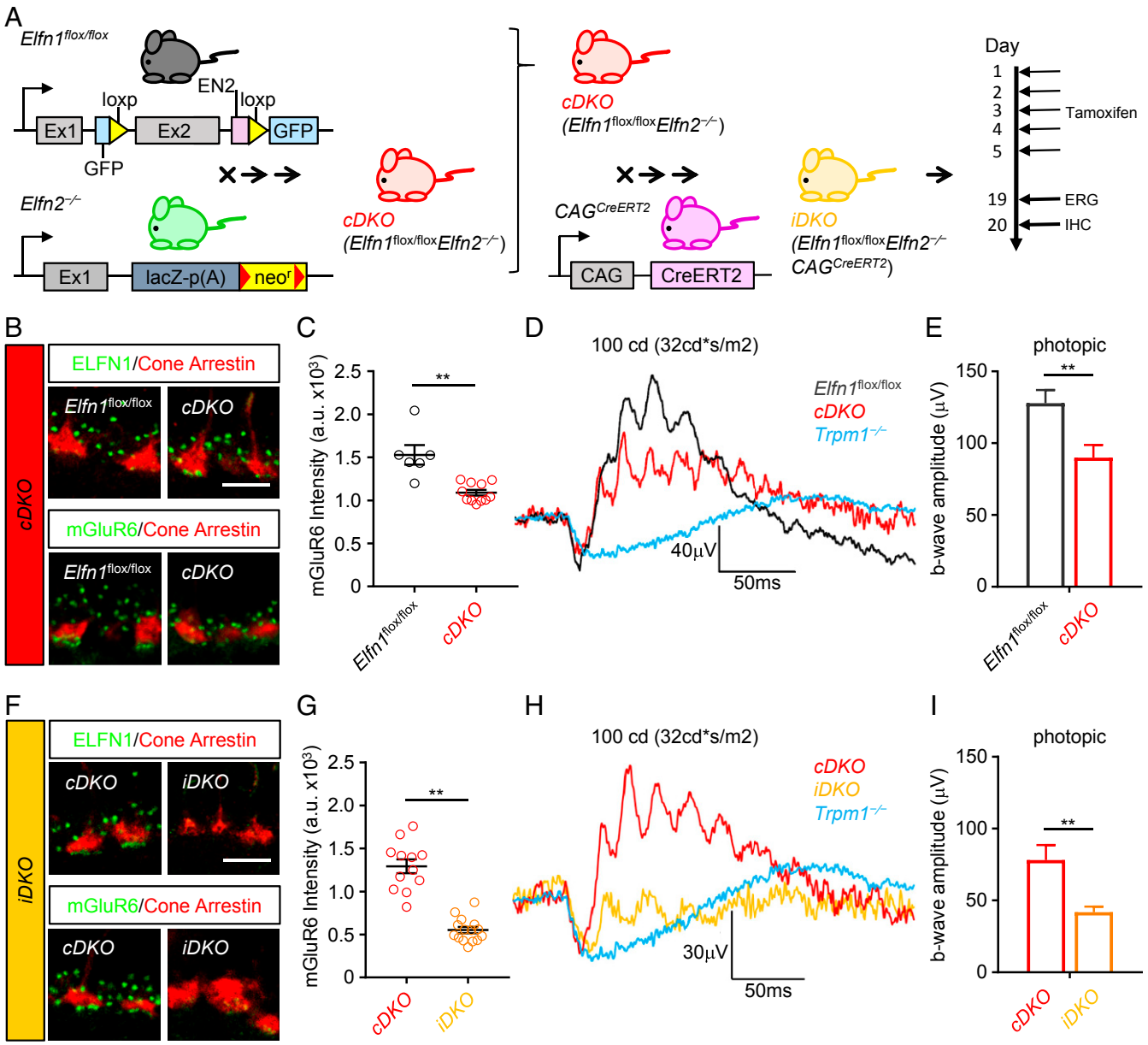

Fig. 6. Reduction of ELFN1 in *Elfn2*$^{-/-}$ mice diminishes cone synaptic transmission. (*A*) Schematic of the strategy for conditional elimination of *Elfn1* in the retina. A conditional knockout allele for *Elfn1* (*Elfn1*$^{flox/flox}$) was generated by flanking exon 2 with loxP sites. *Elfn1*$^{flox/flox}$ mice were crossed with *Elfn2*$^{-/-}$ mice to generate conditional *Elfn1*$^{flox/flox}$*Elfn2*$^{-/-}$ double-knockout mice. *cDKO* mice were then crossed to a tamoxifen-inducible Cre strain to generate inducible double-knockout mice *Elfn1*$^{flox/flox}$*Elfn2*$^{-/-}$*CAG*^{CreERT2}. To induce ELFN1 loss, *iDKO* mice were administered tamoxifen for 5 d followed by testing. IHC, immunohistochemistry. (*B*) Analysis of ELFN1 and mGluR6 localization in cones of *cDKO* mice. Retina cross-sections were double-immunostained with antibody against ELFN1 (green), or mGluR6 (green) and cone terminal marker cone arrestin (red). (Scale bar, 5 μm.) (*C*) Quantification of mGluR6 content in cone synapses of *cDKO* mice. Mean fluorescence intensity from 10 puncta per retina section was measured from three to six sections per retina collected from two separate mice. Data are represented as mean ± SEM; $n = 6$ to 11. $^{**}P < 0.01$, *t* test. (*D*) Analysis of cone synaptic transmission in *cDKO* mice by ERG. Representative traces of responses to a photopic flash of 100 cd*s/m^2 (~58,000 R* per rod) under a 32 cd*s/m^2 (~18,500 R* per rod per second) light background to activate cone pathway only are shown. (*E*) Quantification of b-wave ERG amplitudes in *Elfn1*$^{flox/flox}$ ($n = 5$) and *cDKO* ($n = 6$) mice under photopic conditions. $^{**}P < 0.01$, *t* test. (*F*) Analysis of ELFN1 and mGluR6 localization in cones of *iDKO* mice. Retina cross-sections were double-immunostained with antibody against ELFN1 (green), or mGluR6 (green) and cone terminal marker cone arrestin (red). (Scale bar, 5 μm.) (*G*) Quantification of mGluR6 content in cone synapses of *iDKO* mice. Mean fluorescence intensity from 10 puncta per retina section was measured from three to six sections per retina collected from two separate mice. Data are represented as mean ± SEM; $n = 12$ to 15. $^{**}P < 0.01$, *t* test. (*H*) Analysis of cone synaptic transmission in *iDKO* mice by ERG. Representative traces of responses to a photopic flash of 100 cd*s/m^2 (~58,000 R* per rod) under a 32 cd*s/m^2 (~18,500 R* per rod per second) light background to activate the cone pathway only are shown. (*I*) Quantification of b-wave ERG amplitudes in *cDKO* ($n = 6$) in comparison with *iDKO* ($n = 4$) mice. Data are represented as mean ± SEM. $^{**}P < 0.01$, *t* test.

Discussion

The results of this study offer molecular insight into a long-standing question of how cone photoreceptors wire into the retina circuitry to enable transmission of light-evoked signals. Key to this process is the ability of cones to relay high-sensitivity signals via selective synaptic contacts with many subtypes of ON-CBCs. The response characteristics of the ON-CBCs to cone inputs vary across subtypes, contributing to decoding temporal

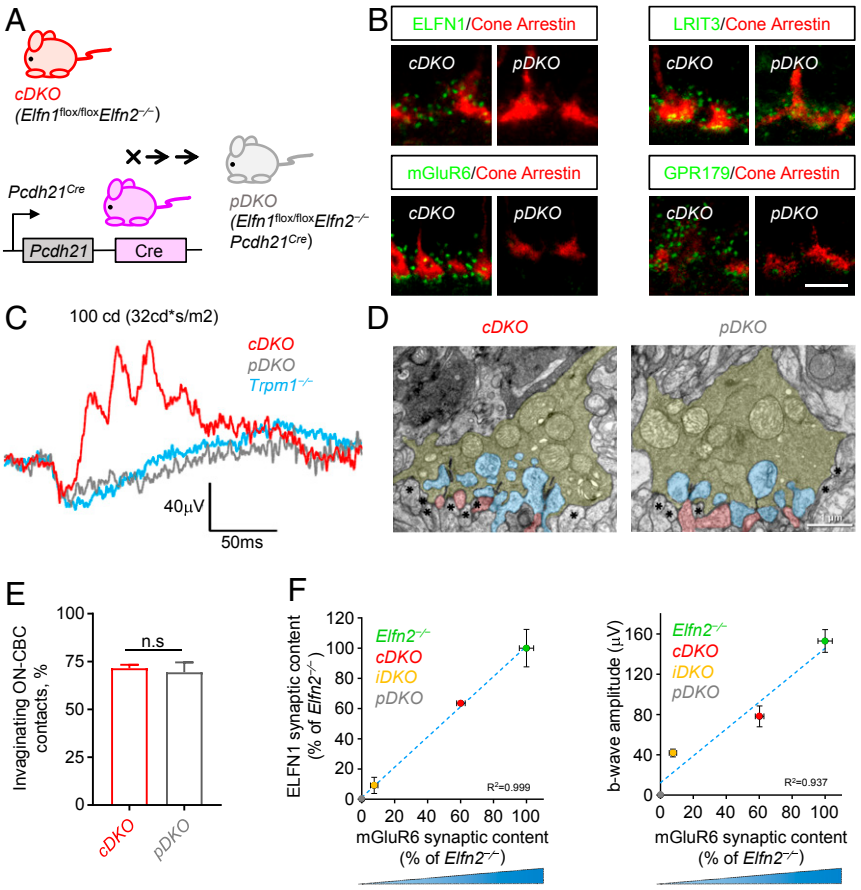

Fig. 7. Elimination of ELFN1 and ELFN2 abolishes synaptic transmission of cones. (*A*) Schematic of the strategy for complete elimination of ELFN1 and ELFN2 in photoreceptors. Conditional *Elfn1*$^{flox/flox}$*Elfn2*$^{-/-}$ *cDKO* mice were crossed with photoreceptor-specific Cre driver line Pcdh21-Cre to generate *Elfn1*$^{flox/flox}$*Elfn2*$^{-/-}$*Pcdh21*^{Cre} mice. (*B*) Analysis of synaptic protein localization in cones of *pDKO* mice. Retina cross-sections were double-immunostained with antibody against ELFN1 (green), mGluR6 (green), GPR179 (green), or LRIT3 (green) with presynaptic cone terminal marker cone arrestin (red). (Scale bar, 5 μm.) (*C*) Analysis of cone photoreceptor synaptic transmission in *pDKO* mice by ERG analysis. Representative ERG traces of responses to a photopic flash of 100 cd*s/m^2 (~58,000 R* per rod) under a 32 cd*s/m^2 (~18,500 R* per rod per second) light background to activate the cone pathway only. (*D*) Examination of cone synaptic morphology by electron microscopy. Photoreceptor axonal terminals are colored in yellow, processes of horizontal cells are in blue, ON-BC dendrites are in pink, and flat-contacting dendrites of cone OFF-BCs are marked with asterisks. (Scale bar, 1 μm.) (*E*) Quantification of synaptic contacts of cone terminals with ON-CBCs; 40 to 60 cone terminals from two separate mice were analyzed for each genotype. Data are represented as mean ± SEM. Mann–Whitney *U* test revealed no significant changes (ns), $P > 0.05$. (*F*) Correlation of mGluR6 content at cone terminals with synaptic ELFN1 and b-wave ERG amplitudes. Quantification of data presented in Figs. 4 *J* and *I*, 6 *B*, *E*, *F*, and *I*, and 7 *B* and *C*.

aspects of vision (21). However, processing of cone signals invariably relies on a sign-inverting metabotropic cascade on all ON-CBCs nucleated by the postsynaptic receptor mGluR6 (22). In this study, we identify the key molecular factors that enable synaptic communication of cones with ON-CBCs. We report that the process is orchestrated by a pair of cell-adhesion molecules, ELFN1 and ELFN2, which act during different stages in development to transsynaptically recruit and maintain mGluR6 in ON-CBC synapses. This mechanism shows important similarities and distinctions from the analogous wiring of rod photoreceptors with their downstream partners, RBCs. First, rods utilize a single molecule, ELFN1, throughout their ontogeny and its elimination selectively affects only rod synapses. Instead, cones express ELFN1 during early synaptogenesis and then switch to cone-specific ELFN2 to support synaptic signaling in mature retinas. Knockout of either ELFN1 or ELFN2 alone does not prevent their signaling to ON-CBCs due to the apparently compensatory relationship between the two molecules. Second, like ELFN1, in adult retinas the new player ELFN2 directly interacts with mGluR6, stabilizing it at the tips of ON-CBC dendrites. Third, interaction with ELFN1 and ELFN2 clearly regulates pharmacological properties of mGluR6 in trans, thus contributing to responses of ON-BCs to glutamate. Fourth, deletion of both ELFN1 and ELFN2 completely prevents synaptic transmission of cones, indicating that the two molecules are sufficient for mGluR6 recruitment and establishing the communication channel. Fifth, in contrast to rods, loss of both ELFN proteins does not prevent cones from making physical contacts with ON-CBCs. This likely reflects a morphologically distinct organization of cone synapses that feature shallow contacts with cone pedicles in contrast to deeply invaginating RBC contacts within rod spherules, while additionally synapsing with rod-avoiding OFF-CBC neurons. We believe that reliance on two synergistically acting cell-adhesion molecules constitutes a synaptic code that at least in part contributes to setting up their unique connectivity pattern and characteristic synaptic properties.

Our observations prompt a few intriguing questions that open new avenues for future explorations. Quintessentially, many of these revolve around diversification of cell-adhesion molecules for anchoring mGluR6 and reliance of cones on both ELFN1 and ELFN2 for development and synaptic signaling. The observation that mature cone synapses exclusively utilize ELFN2 while in principle ELFN1 can seemingly substitute for it suggests that ELFN2 endows cone synapses with some unique features

advantageous for cone function. One such domain could be related to shaping unique temporal or adaptive properties of cone synapses which essentially rely on mGluR6 signaling. We found that ELFN2 can allosterically modulate mGluR6 pharmacology in trans, lowering its affinity for glutamate and decreasing maximal activity. These effects are similar to the ones exerted by ELFN1 (23), yet may be quantitatively distinct and thus could endow distinct synaptic properties to differentiate cone synapses. Even subtle alterations in mGluR6 pharmacological properties would likely have significant impact on how readily and fast ON-BCs respond to changes in glutamate release by the photoreceptors during the light response, thus affecting temporal characteristics of the response and its light sensitivity. Provocatively, it could be imagined that these parameters are adjusted differentially across subtypes of ON-CBCs, further contributing to diversification of their responses. The ERG recordings employed in this study do not have the power to resolve functional differences in response parameters of individual ON-BCs, making it of interest to examine selective contribution of ELFN2 to establishing synaptic properties of various ON-CBC populations in future studies. Alternatively, we can also envision that ELFN2 may endow cones with advantages related to postdevelopmental synaptic maintenance and/or presynaptic function. Previously, we found that ELFN1 is integrated with the presynaptic release apparatus by forming a complex with $\alpha2\delta4/Ca_V1.4$ that regulates transmitter release (24). We expect that, by analogy, ELFN2 is also integrated with the vesicular release machinery in the active zone of cone pedicles. Consistent with this possibility, our observations show that deletion of $Ca_V1.4$ prevents accumulation of ELFN2 in cone pedicles. However, unlike ELFN1, whose synaptic localization in rods depends completely on $\alpha2\delta4$, targeting of ELFN2 to cone synapses is unaffected by the $\alpha2\delta4$ deletion. It suggests the key role of ELFN2 in selective preservation of cone transmission in $\alpha2\delta4$ knockouts and thus the identification of ELFN2 may provide a molecular explanation for the resilience of cone synapses. Moreover, ELFN1 and ELFN2 vary considerably (sharing only 49% identity), making it possible that they differentially affect vesicular release and/or its homeostatic regulation. It also seems possible that ELFN1 could be utilized early in development for the advantages that it provides over ELFN2 in some aspect of morphological development. While we have not detected overt developmental defects in cone synaptogenesis in retinas lacking ELFN1, this possibility may need to be examined in finer detail. The reciprocal sensitivity of ELFN1 and ELFN2 expression levels and distinct profiles of their developmental regulation suggest that the interplay may be important for some, yet to be determined, aspects of retina physiology.

Interestingly, several cell-adhesion molecules with essential roles in regulating transmission to ON-BCs are preferentially enriched in cone synapses. Most notably, these include other members of the leucine-rich repeat (LRR) family, LRIT1 and LRIT3, which share the same domain architecture with ELFN proteins (25–29). Because LRR proteins are well-known to form both homophilic and heterophilic dimers (30, 31), it seems possible that ELFN2 could be uniquely integrated within a larger cone-specific scaffold to regulate their presynaptic properties. Supporting this idea are our observations that LRIT3 and ELFN2 are reciprocally sensitive to the elimination of either. There is an abundant precedent in the literature that members of the LRR family can regulate neurotransmitter release (19, 30–32), making it of interest to explore whether ELFN2 imparts cone pedicles with specific features related to glutamate exocytosis.

Our study also uncovers that the synaptogenesis mechanisms of cone and rod photoreceptors appear to be different. While ELFN1 was strictly required for the establishment of physical contacts between rods and RBCs (17), deletion of both ELFN1 and ELFN2 did not seem to compromise formation of cone synapses with ON-CBCs despite complete loss of synaptic transmission. The mechanistic details for this differential reliance of cones on physical wiring remain unclear. However, we speculate that this may be related to selective synaptic specificity of cones as they establish contacts before rods. Furthermore, cones connect with unique postsynaptic partner OFF-BCs that do not synapse with rods and also largely avoid RBCs. Establishment of this selectivity likely requires orchestrating multiple molecular events to coordinate contact selection and avoidance. As a result, disruption of ELFN proteins only may be insufficient to alter this process.

In addition to providing molecular and mechanistic insight into retina wiring, our study introduces a powerful toolset for genetic control of functional photoreceptor wiring into the visual circuitry. Using combinations of the conditional *Elfn1* knockout allele with *Elfn2*-null and cell-specific Cre-driver lines offers the possibility to selectively disconnect either photoreceptor from transmitting its signals via respective ON-BC channels. Importantly, these manipulations preserve normal receptor physiology and phototransduction, thereby allowing specific dissection of the physiological roles played by individual pathways for the transduction of photoreceptor signals (e.g., primary vs. secondary rod pathway vs. cone OFF, etc.). We believe that these genetic tools may be valuable for dissecting contributions of various pathways transducing light signal to generating retinal output in ganglion cells and programming behavioral responses.

Finally, we think that similar mechanisms based on the interplay of ELFN1 and ELFN2 cell-adhesion molecules may play out across the nervous system, providing cell-specific recruitment and modulation of G protein-coupled receptors (GPCRs) to synapses with differential developmental trajectories. Indeed, transsynaptic allosteric modulation of GPCRs represents an emerging dimension in our understanding of synaptic neurotransmission (33). Although much remains to be learned about ELFN2 mechanisms and the interplay with ELFN1, both proteins show differential and partially overlapping expression patterns across various neuronal populations in the brain (19). Furthermore, in some synapses, deletion of ELFN1 alone was sufficient for disrupting transsynaptic mGluR recruitment (34, 35) and the interplay in neurons expressing both is envisioned. Elucidating their relative contributions to the organization of metabotropic synapses and the mGluR group III system is an exciting direction prompted by the current study.

Materials and Methods

Methods performed in the current study involved generation of DNA constructs, cell culture, subretinal injections, immunoprecipitation, GPCR signaling assays, in situ hybridization, immunohistochemistry, electroretinography, and electron microscopy. Briefly, Elfn2 was virally expressed in the retina with rAAV constructs driven by the PR2.1 promoter. Retinas from various species were harvested and lysed and proteins extracted with 1% Triton X-100 were immunoprecipitated with anti-mGluR6 antibodies. For the transient transfection, HEK293T cells were used. In addition to mGluR6, cells were transfected with sensor constructs (-22F cAMP pGloSensor, Nluc-EPAC-VV or Venus 156-239-Gβ1, Venus 1-155-Gγ2, and masGRK3ctNluc) and signal was monitored in real time upon the addition of L-AP4 and glutamate. Cell specificity of Elfn2 expression was established by in situ hybridizations using probes corresponding to the Elfn2 sequence and a marker for cones, Gnat2. To establish protein localization, immunohistochemistry was used, staining retina cross-sections with the primary antibodies of choice followed by the corresponding secondary antibodies. Image acquisition and processing were accomplished using ZEN 2011 and Amira software packages. Electroretinography was performed on anesthetized mice. Full-field white flashes were produced by a set of light-emitting diodes. Traces were recorded from corneal electrodes and analyzed using electron microscopy LKC Technologies software. For electron microscopy, retina eyecups were fixed in 2% osmium tetroxide for 1 h, en block-stained with 1% uranyl acetate, and imaged on a Tecnai G2 Spirit BioTwin (FEI) transmission electron microscope at 80 or 100 kV accelerating voltage. All procedures involving mice were carried out in accordance with NIH guidelines and approved by the Institutional Animal Care And Use Committees. Additional details for these procedures are available in *SI Appendix*.

Data Availability. All study data are included in the article and *SI Appendix*.

ACKNOWLEDGMENTS. We thank Ms. Natalia Martemyanova for performing genetic crosses needed to obtain the mice utilized in these studies. We thank the Light Microscopy Core at the Max Planck Florida Institute for Neuroscience for supporting image acquisition. This work was supported by NIH Grants EY018139 and EY028033 (to K.A.M.) and K99EY030554 (to Y.W.), the National Eye Institute Intramural Research Program (W.L.), French Muscular Dystrophy Association (AFM-Téléthon), Retina France, UNADEV-Aviesan call 2015, Institut Hospitalo-Universitaire FOReSIGHT (ANR-18-IAHU-0001), and French state funds managed by the Agence Nationale de la Recherche within the Investissements d'Avenir program (to C.Z.).

1. L. B. Vosshall, M. Carandini, Sensory systems. *Curr. Opin. Neurobiol.* **19**, 343–344 (2009).
2. E. R. Kandel, J. H. Schwartz, T. M. Jessell, *Principles of Neural Science*, (McGraw-Hill, ed. 4, 2000).
3. O. Sporns, G. Tononi, G. M. Edelman, Connectivity and complexity: The relationship between neuroanatomy and brain dynamics. *Neural Netw.* **13**, 909–922 (2000).
4. G. T. Meijer, P. E. C. Mertens, C. M. A. Pennartz, U. Olcese, C. S. Lansink, The circuit architecture of cortical multisensory processing: Distinct functions jointly operating within a common anatomical network. *Prog. Neurobiol.* **174**, 1–15 (2019).
5. T. D. Lamb, Evolution of phototransduction, vertebrate photoreceptors and retina. *Prog. Retin. Eye Res.* **36**, 52–119 (2013).
6. M. Hoon, H. Okawa, L. Della Santina, R. O. Wong, Functional architecture of the retina: Development and disease. *Prog. Retin. Eye Res.* **42**, 44–84 (2014).
7. D. G. Luo, T. Xue, K. W. Yau, How vision begins: An odyssey. *Proc. Natl. Acad. Sci. U.S.A.* **105**, 9855–9862 (2008).
8. V. J. Kefalov, Rod and cone visual pigments and phototransduction through pharmacological, genetic, and physiological approaches. *J. Biol. Chem.* **287**, 1635–1641 (2012).
9. T. D. Lamb, Why rods and cones? *Eye (Lond.)* **30**, 179–185 (2016).
10. N. T. Ingram, A. P. Sampath, G. L. Fain, Why are rods more sensitive than cones? *J. Physiol.* **594**, 5415–5426 (2016).
11. M. E. Burns, V. Y. Arshavsky, Beyond counting photons: Trials and trends in vertebrate visual transduction. *Neuron* **48**, 387–401 (2005).
12. K. W. Yau, R. C. Hardie, Phototransduction motifs and variations. *Cell* **139**, 246–264 (2009).
13. J. I. Korenbrot, Speed, sensitivity, and stability of the light response in rod and cone photoreceptors: Facts and models. *Prog. Retin. Eye Res.* **31**, 442–466 (2012).
14. J. R. Sanes, M. Yamagata, Many paths to synaptic specificity. *Annu. Rev. Cell Dev. Biol.* **25**, 161–195 (2009).
15. J. S. Mumm *et al*., Laminar circuit formation in the vertebrate retina. *Prog. Brain Res.* **147**, 155–169 (2005).
16. S. H. DeVries, D. A. Baylor, Synaptic circuitry of the retina and olfactory bulb. *Cell* **72**, 139–149 (1993).
17. Y. Cao *et al*., Mechanism for selective synaptic wiring of rod photoreceptors into the retinal circuitry and its role in vision. *Neuron* **87**, 1248–1260 (2015).
18. D. Kerschensteiner, J. L. Morgan, E. D. Parker, R. M. Lewis, R. O. Wong, Neurotransmission selectively regulates synapse formation in parallel circuits in vivo. *Nature* **460**, 1016–1020 (2009).
19. H. A. Dunn, S. Zucca, M. Dao, C. Orlandi, K. A. Martemyanov, ELFN2 is a postsynaptic cell adhesion molecule with essential roles in controlling group III mGluRs in the brain and neuropsychiatric behavior. *Mol. Psychiatry* **24**, 1902–1919 (2019).
20. M. T. Pardue, N. S. Peachey, Mouse b-wave mutants. *Doc. Ophthalmol.* **128**, 77–89 (2014).
21. T. Ichinose, B. Fyk-Kolodziej, J. Cohn, Roles of ON cone bipolar cell subtypes in temporal coding in the mouse retina. *J. Neurosci.* **34**, 8761–8771 (2014).
22. K. A. Martemyanov, A. P. Sampath, The transduction cascade in retinal ON-bipolar cells: Signal processing and disease. *Annu. Rev. Vis. Sci.* **3**, 25–51 (2017).
23. H. A. Dunn, D. N. Patil, Y. Cao, C. Orlandi, K. A. Martemyanov, Synaptic adhesion protein ELFN1 is a selective allosteric modulator of group III metabotropic glutamate receptors in trans. *Proc. Natl. Acad. Sci. U.S.A.* **115**, 5022–5027 (2018).
24. Y. Wang *et al*., The auxiliary calcium channel subunit alpha2delta4 is required for axonal elaboration, synaptic transmission, and wiring of rod photoreceptors. *Neuron* **93**, 1359–1374.e6 (2017).
25. I. Sarria *et al*., LRIT1 modulates adaptive changes in synaptic communication of cone photoreceptors. *Cell Rep.* **22**, 3562–3573 (2018).
26. A. Ueno *et al*., Lrit1, a retinal transmembrane protein, regulates selective synapse formation in cone photoreceptor cells and visual acuity. *Cell Rep.* **22**, 3548–3561 (2018).
27. M. Neuillé *et al*., Lrit3 deficient mouse (nob6): A novel model of complete congenital stationary night blindness (cCSNB). *PLoS One* **9**, e90342 (2014).
28. M. Neuillé *et al*., LRIT3 is essential to localize TRPM1 to the dendritic tips of depolarizing bipolar cells and may play a role in cone synapse formation. *Eur. J. Neurosci.* **42**, 1966–1975 (2015).
29. N. Hasan *et al*., Presynaptic expression of LRIT3 transsynaptically organizes the postsynaptic glutamate signaling complex containing TRPM1. *Cell Rep.* **27**, 3107–3116.e3 (2019).
30. J. Ko, E. Kim, Leucine-rich repeat proteins of synapses. *J. Neurosci. Res.* **85**, 2824–2832 (2007).
31. J. de Wit, W. Hong, L. Luo, A. Ghosh, Role of leucine-rich repeat proteins in the development and function of neural circuits. *Annu. Rev. Cell Dev. Biol.* **27**, 697–729 (2011).
32. E. L. Sylwestrak, A. Ghosh, Elfn1 regulates target-specific release probability at CA1-interneuron synapses. *Science* **338**, 536–540 (2012).
33. H. A. Dunn, C. Orlandi, K. A. Martemyanov, Beyond the ligand: Extracellular and transcellular G protein-coupled receptor complexes in physiology and pharmacology. *Pharmacol. Rev.* **71**, 503–519 (2019).
34. N. H. Tomioka *et al*., Elfn1 recruits presynaptic mGluR7 in trans and its loss results in seizures. *Nat. Commun.* **5**, 4501 (2014).
35. T. J. Stachniak, E. L. Sylwestrak, P. Scheiffele, B. J. Hall, A. Ghosh, Elfn1-induced constitutive activation of mGluR7 determines frequency-dependent recruitment of somatostatin interneurons. *J. Neurosci.* **39**, 4461–4474 (2019).